11^{th} International Conference on Fracture Mechanics of Concrete and Concrete Structures
FraMCoS-11
J. M. Chandra Kishen, A. Ramaswamy, S. Ray and R. Vidyasagar (Eds)
https://doi.org/10.21012/FC11.092368

FRACTURE CHARACTERIZATION OF 3D -PRINTED ULTRA-HIGH PERFORMANCE FIBER CONCRETE BEAMS USING ACOUSTIC EMISSION

VIGNESH K. RAMAMURTHY*, PRABHAT R. PREM†, VAIBHAV V. INGLE * and GREESHMA GIRIDHAR *

*Research Fellow, CSIR-Structural Engineering Research Centre, Chennai 600 113, India.

†Principal Scientist, CSIR-Structural Engineering Research Centre, Chennai 600 113, India.
e-mail: prabhat@serc.res.in

Key words: 3D Concrete Printing, UHPC, Fiber, Fracture, Acoustic Emission.

Abstract. The present study utilizes Acoustic Emission (AE) Testing to investigate the fracture process in 3D Printed-Ultra High-Performance Concrete (3DP-UHPC) beams under three-point bending. These 3D printed UHPC specimens are reinforced with micro steel fibers at a dosage of 2% by volume and feature two distinct notch depths, 6 mm and 60 mm. During the testing process, AE is employed to evaluate the fracture process zone and transition ligament length (a_l) of the prisms. The Work of fracture method and the Boundary Effect method is employed to determine both Size-Dependent (G_f) and Size Independent Fracture energies (G_F).

1 INTRODUCTION

In the last two decades construction industry witness the adoption of automotive technology with the efforts of many researchers, academicians, and industrialists worldwide. Incorporating existing additive techniques in the construction sector gives a new arena with benefits such as enhanced geometric flexibility, less human labor, cost and time, and minimal risk. Three-dimensional (3D) printing is a revolutionary additive manufacturing technique that has found diverse applications across industries, offering the advantage of rapid production of complex structures while reducing waste, labor costs, and production time. Despite its immense potential, most existing studies on 3D printed concrete have primarily focused on aspects like rheology, buildability, compression, tension, shear performance, layer-interface properties, fiber enhancement, stress-strain curves, failure models, and simulation methods. Surprisingly, there remains a significant gap in research regarding the fracture characteristics of 3D-printed concrete [1]. Understanding the fracture behavior of 3D-printed concrete is paramount, as this material exhibits quasi-brittle characteristics and is susceptible to fracturing under mechanical and environmental loads. Several key factors in 3D printing concrete influence fracture behavior, such as printing path, time intervals between layers, and fresh state rheological characteristics of the material. Understanding how these factors impact fracture characteristics like energy and the toughness of 3D-printed concrete is essential for designing resilient and durable structures. However, despite extensive efforts and successful modeling of fracture behavior, our quantitative understanding of the physical processes that ultimately control fracture remains weak. While some prediction of failure loads and damage patterns is possible, a fundamental understanding of the same is lack-

ing. Bridging this knowledge gap would enable the development of predictive models for large-scale structural performance and reliability, with microstructure-performance connections serving as the key to true material understanding [2, 3]. In pursuit of this understanding, experiments have been conducted to establish a link between the energy released at the microscale and the bulk fracture energy measured globally. In the current study, authors investigate the fracture energy of 3DP-UHPC beams using AE testing. AE methods have been utilized to observe the energy release on a microscopic scale. The AE signals generated during micro-cracking and fracture stages offer valuable insights into the fracture processes of tested objects. By analyzing AE signal's onset times and characteristics, valuable information about fracture behavior can be obtained [4, 5].

2 METHODOLOGY

2.1 Mix design and Printing

In this research study, a gantry-type 3D printer is employed to fabricate 3DP-UHPC prisms. To simplify the printing procedure, an extruder of a cylindrical shape is connected to the printer's lever arm through an augur-motor system. This integration allows for a more efficient and streamlined printing process. The entire printing operation is orchestrated using a design toolpath generated through G-code, ensuring accurate and efficient movement of the printer's components. The extrusion process involves utilizing a nozzle with a diameter of 20 mm, and the material is pushed through this nozzle at a printing speed of 60 mm/s. This printing speed represents the rate at which the material is deposited and forms the desired structure or shape in the additive manufacturing process. Using a larger nozzle and relatively high print speed allows for faster production of the desired objects or components, making the manufacturing process more efficient. However, it is important to ensure that the chosen material is compatible with the specific printing parameters to achieve the desired quality and mechanical properties in the final product. Proper consideration of the material's flow characteristics and temperature control is crucial to avoid issues such as clogging or uneven extrusion. The extrudability and buildability of the material are assessed using qualitative analysis, while workability and shape-retention ability are measured through experimental quantification. In the current study, the concrete mix comprises various binders in specific proportions of 76% cement, 1% limestone powder, 17% fly ash, 6%, and silica fume. The supplementary cementitious material in the designed mix decreases the heat of hydration and enhances the long-term properties of the designed mix, resulting in improved durability and performance. A PCE-based superplasticizer with a dosage of 0.7% of the binder content by weight is added to the mix to optimize workability. This admixture effectively enhances the fluidity and ease of handling during construction. The w/c ratio is carefully maintained at 0.23 to achieve the desired consistency and strength. The sand used in the mix have a particle size of less than 2mm, contributing to the overall cohesiveness of the concrete. Additionally, to reinforce the concrete and enhance its tensile strength and resistance to cracking, 13 mm long steel fibers are incorporated into the mix. More details about the chemical composition of the materials and mix design are detailed in [6, 7].

2.2 Testing and instrumentation

The experimental configuration of notched prisms loaded under three-point bending is depicted in Fig 1. The experiments use displacement control with a loading rate set at 0.05 mm/min. The beams are tested until their softening behavior becomes evident. An 8-Channel PCI-Express Bus AE system is employed as the measuring system. A total of six R6I-AST sensors are employed in the study. These sensors have a peak sensitivity of 117 dB, with a frequency range spanning from 40 kHz to 95 kHz. These sensors are securely mounted on the specimen surface to detect and record AE signals, using silicone grease for coupling. The

pre-amplifier gain is set to 40 dB. The sensitivity and coupling of the AE sensors are determined using a Hsu-Nielsen source (pencil-lead break). A similar strategy is adopted in previous studies [4, 5].

Figure 1: Typical test set up

3 Results and Discussion

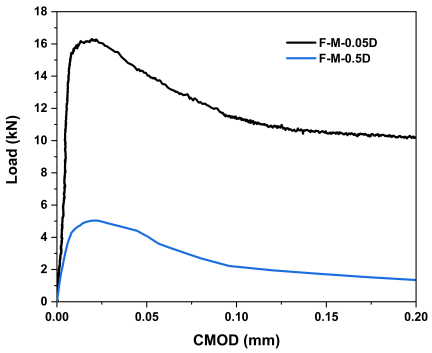

Figure 2: Fracture response of tested specimens

Fig 2 shows the fracture response of notched 3DP-UHPC beams. It is clear that a 6mm notched beam shows a greater stiffness compared to a 60mm notched beam. The CMOD of the tested specimens could not be continued until the failure of specimens due to the limitation of the gauge length. Using the AE technique, the fracture behavior of 3DP-UHPC prisms is correlated with acoustic emission parameters like AE Energy and AE events during pre-peak and post-peak stages in Fig 2. Previous studies [10] demonstrate that AE activity like AE events, AE energy found to be higher during the post-peak regime while the pre-peak regime shows minimal activity. The G_F is determined considering the post-peak regime, using parameters like ligament length a_l and notch length, which are discussed in further sections below.

3.1 AE energy

AE energy is the rapid release of energy resulting from the initiation and propagation of micro-cracks under three-point bending. AE activity is found to be higher during the post-peak stage since a significant amount of micro-cracks are generated in the notched prism, exhibiting higher energy dissipation in the post-peak stage. In various instances [10, 14–16], a correlation may exist between the cumulative AE energy and the fracture energy.

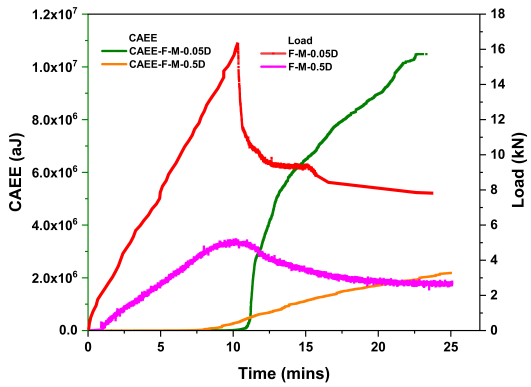

Figure 3: AE response of notched 3D-UHPC prisms

As the material undergoes deformation and microcracking, the cumulative AE energy will generally increase, signifying the progressive damage in the material. In ductile materials, this damage accumulation is often associated with increased fracture energy, indicating the material's ability to undergo plastic deformation and absorb energy before failure. Based

on the observations from Fig 3, it is clear that during the testing of 3DP-UHPC specimens, the cumulative AE energy for the FM-0.05D configuration shows a higher energy dissipation of nearly $1.1 * 10^7$ aJ compared to the FM-0.5D configuration of $2 * 10^6$ aJ. Additionally, it is found that the FM-0.05D specimen exhibits a higher load-carrying capacity in the range of 16 kN, which can be attributed to its lower notch depth, while the FM-0.5D specimen demonstrates a lesser load-carrying capacity of 5 kN due to its higher notch depth. The higher cumulative AE energy in the FM-0.05D configuration indicates that more AE signals were detected during the deformation and failure process. This suggests that the FM-0.05D specimen underwent more damage accumulation, microcracking, and energy dissipation compared to the FM-0.5D specimen. The increased energy dissipation in the FM-0.05D specimen is likely due to the presence of a shallower notch, which led to a more gradual and ductile failure process, allowing the material to absorb and dissipate more energy before complete failure.

3.2 AE Events

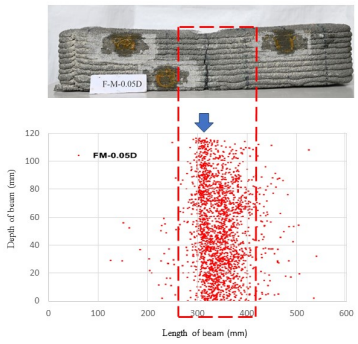

Figure 4: Typical comparison of AE events versus failure pattern of 3DP- UHPC prism having notch depth of 6 mm

AE events are associated with various damage mechanisms, including crack initiation, propagation, and microcracking due to the generation of transient elastic waves ie, acoustic signals by a material. In fracture behavior testing of 3DP-UHPC notched specimens, events play a significant role in determining G_F as the a_l is found from the histogram of AE events shown in Fig 6 and Fig 7. The source localization of cracks or damage formed is also determined while testing 3DP-UHPC notched specimens as shown in Fig 4 and Fig 5. Significantly more events are generated in the notch zone for 6mm notched prisms compared to 60mm notched prisms due to higher stress concentration in lower notch depths.

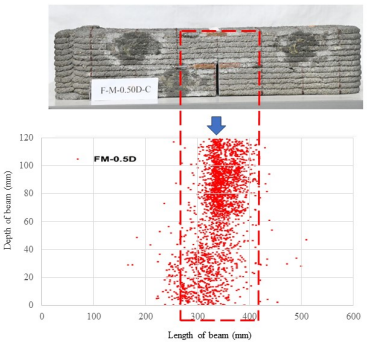

Figure 5: Typical comparison of AE events versus failure pattern of 3DP-UHPC prism having notch depth of 60 mm

3.3 Fracture characteristics using AE

3.3.1 Transition Ligament length (a_l)

a_l refers to the critical ligament length at which fracture behavior transitions occur. It is the point at which the material transitions from stable crack growth to unstable crack propagation leading to failure. The G_F is obtained by examining the relationship between a_l and AE events via histogram plot. This method offers an alternative approach to computing the fracture energy without needing the least squares method and handling over-determined systems of equations when using data from multiple specimens [17]. Abdalla and Karihaloo [13] observed that the transition ligament length initially increased as the specimen size increased, but this increase occurred at a diminishing rate. The transition ligament length stabilized after

reaching a certain point, showing little to no further increase with larger specimens. To assess the parameter a_l, the acoustic emission (AE) sources are graphically represented in relation to the depth of the specimen (y), illustrated in Fig 6 and Fig 7 and compared with the tested specimens in Fig 4 and Fig 5. In order to evaluate Fracture Process Zone (FPZ) width, the AE sources are plotted with respect to the length of specimen(X). In this study, it is evident that transition length a_l is higher (40mm) for notch size 6mm while lesser length a_l (20mm) is observed for notch size 60mm as shown in event histograms.

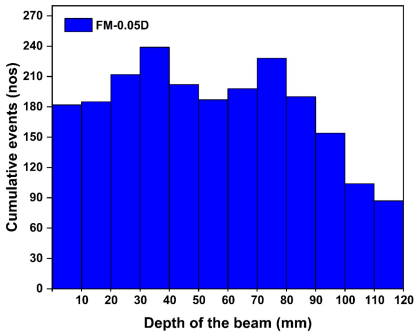

Figure 6: Cumulative AE events versus depth of 3DP-UHPC prism having notch depth of 6 mm

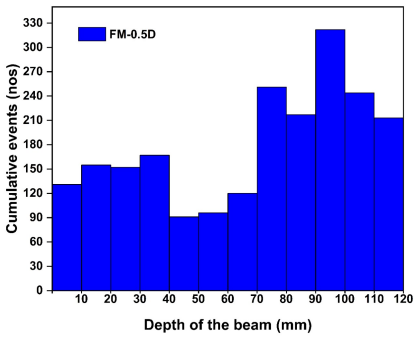

Figure 7: Cumulative AE events versus depth of 3DP-UHPC prism having notch depth of 60 mm

3.3.2 Size-independent fracture energy (G_F)

In earlier studies, the estimation of G_F is carried out using the bilinear boundary effect model [9] and trilinear model [10] in combination with AE data. The trilinear model offers a more refined representation of energy distribution along the ligament length compared to the bilinear model under the three-point bending of specimens and found that it is more precise. Bazant et al. [11] introduced an innovative size effect model that differs from the conventional approach using three specimen sizes. Their method suggests that employing just one specimen size is adequate to determine fracture parameters. Tang et al. [12] demonstrated that fracture parameters can be promptly obtained through this variable notch one-size method approach. In the current study, the fracture energy (G_f) is determined by computing the area under the load-displacement curve and accounting for the self-weight compensation term using the work-of-fracture method. The mathematical expression for calculating G_f is given in Eq. 1. In Eq. 1 B, D, a_o, mg, δ_{max} denote thickness, depth, notch depth, self-weight, and maximum vertical displacement of the prism, respectively.

$$G_f = \frac{\int_0^{\delta_{\max}} P d\delta + \mathrm{mg}\delta_{\max}}{B\left(D - a_0\right)} \tag{1}$$

From Eq 1, $G_f$is calculated as 207 N/m for FM-0.05D (6mm) and 81.4 N/m for FM-0.5D (60mm). Furthermore, the G_F is evaluated based on the Bilinear model given in Eq. 2. This model gives G_F estimation by accounting between the free boundary surface and the FPZ. In Eq. 2 a, a_l, G_F, G_f specify notch length, transition ligament length, size-independent fracture energy and specific fracture energy respectively.

$$G_F\left(\frac{a}{d}\right) = \begin{cases} G_f\left[1 - \frac{1}{2}\frac{\frac{a_l}{d}}{1-\frac{a}{d}}\right] & 1 - \frac{a}{d} > \frac{a_l}{d} \\ G_f \frac{1}{2}\frac{\left(1-\frac{a}{d}\right)}{\frac{a_l}{d}} & 1 - \frac{a}{d} \leq \frac{a_l}{d} \end{cases} \tag{2}$$

On further samplification from Eq 2, G_F is calculated as 171.20 N/m for FM-0.05D (6mm)

and 67.8 N/m for FM-0.5D (60mm). In table 1 the obtained values of G_f, G_F and a_l is presented for varying notch sizes.

Table 1: G_f, G_F of varying notch size

Description	F-M- 0.05D	F-M-0.5D
Size (mm)	120 x 120 x 600	120 x 120 x 600
Notch Depth (mm)	6	60
Transition ligament length (mm)	40	20
G_f (N/m)	207	81.4
G_F (N/m)	171.20	67.8

4 Conclusion

The present research focuses on studying the fracture characteristics of 3DP-UHPC notched prisms using three-point bending and AE testing. Two fracture energy evaluation methods, namely the work of fracture method and boundary effect method, are employed to analyze the G_f and G_F of the specimens, respectively. The study reveals that as the notch depth increases, the transition ligament length a_l diminishes, subsequently causing a decrease in both the G_f and G_F (size-independent fracture energy) of the 3DP-UHPC prisms. The size-independent fracture energy is more than double the size-dependent fracture energy. Moreover, it is observed that the ligament length of 6 mm notch specimens is twice that of 60 mm notched specimens. Extensive studies to determine the fracture behavior of 3DP-UHPC specimens are currently underway, and the findings will be reported in future publications.

REFERENCES

[1] Kaliyavaradhan, S. K., Ambily, P. S., Prem, P. R., & Ghodke, S. B. (2022). Test methods for 3D printable concrete. Automation in Construction, 142, 104529.

[2] Nair, S. A., Panda, S., Santhanam, M., Sant, G., & Neithalath, N. (2020). A critical examination of the influence of material characteristics and extruder geometry on 3D printing of cementitious binders. Cement and Concrete Composites, 112, 103671.

[3] Yang, Y., Wu, C., Liu, Z., Wang, H., & Ren, Q. (2022). Mechanical anisotropy of ultra-high performance fibre-reinforced concrete for 3D printing. Cement and Concrete Composites, 125, 104310.

[4] Prem, P. R., Murthy, A. R., & Verma, M. (2018). Theoretical modelling and acoustic emission monitoring of RC beams strengthened with UHPC. *Construction and Building Materials*, 158, 670-682.

[5] Prem, P. R., Verma, M., & Ambily, P. S. (2021, April). Damage characterization of reinforced concrete beams under different failure modes using acoustic emission. Structures Vol. 30, pp. 174-187.

[6] Greeshma Giridhar, Prabhat Ranjan Prem & Shankar Kumar . 2023. Development of concrete mixes for 3D printing using simple tools and techniques *Sadhana*

[7] Ravichandran, D., Giridhar, G., kumar Ramamurthy, V., & Prem, P. R. (2023). Influence of test protocol on determining the rheological properties of cement pastes mixtures for concrete 3D printing.

[8] Xie, C., Cao, M., Khan, M., Yin, H., & Guan, J. (2021). Review on different testing methods and factors affecting fracture properties of fiber reinforced cementitious composites. Construction and Building Materials, 273, 121766.

[9] Hu, X., & Wittmann, F. (2000). Size effect on toughness induced by crack close to free surface. Engineering fracture mechanics, 65(2-3), 209-221.

[10] Muralidhara, S., Prasad, B. R., Karihaloo, B. L., & Singh, R. K. (2011). Size-independent fracture energy in plain concrete beams using tri-linear model. Con-

struction and Building Materials, 25(7), 3051-3058.

[11] Bažant, Z. P., & Li, Z. (1996). Zero-brittleness size-effect method for one-size fracture test of concrete. Journal of engineering mechanics, 122(5), 458-468.

[12] Tang, T., Yang, S., & Zollinger, D. G. (1999). Determination of Fracture Energy and Process Zone Length by Using Variable-Notch One-Size Specimens. Materials Journal, 96(1), 3-10.

[13] Abdalla, H. M., & Karihaloo, B. L. (2003). Determination of size-independent specific fracture energy of concrete from three-point bend and wedge splitting tests. Magazine of concrete research, 55(2), 133-141.

[14] Landis, E. N., & Baillon, L. (2002). Experiments to relate acoustic emission energy to fracture energy of concrete. Journal of engineering mechanics, 128(6), 698-702.

[15] Otsuka, K., & Date, H. (2000). Fracture process zone in concrete tension specimen. Engineering fracture mechanics, 65(2-3), 111-131.

[16] Raghu Prasad, B. K.,& Vidya Sagar, R. (2008). Relationship between AE energy and fracture energy of plain concrete beams: experimental study. Journal of Materials in Civil Engineering, 20(3), 212-220.

[17] Alam, S. Y., Saliba, J., & Loukili, A. (2014). Fracture examination in concrete through combined digital image correlation and acoustic emission techniques. Construction and Building Materials, 69, 232-242.